1st International Conference for Geotechnical Engineering and Transportation ICGTE in24-15/4/2013

Consolidation Behavior of Two-Pile Group System under Different Loading Condition Using the Bounding Surface Model

Dr. Qassun S. Mohammed Shafiqu
Civil Engineering Department, Al-Nahrain University/ Iraq
Email: qassun@yahoo.com
Maarib M. Ahmed.
Civil Engineering Department, Al-Nahrain University/ Iraq

ABSTRACT

In this paper, soil-water coupling analyses with finite element method are conducted to investigate the long-term displacements of two-pile foundation installed in saturated cohesive soils under different loading condition. As constitutive model for clayey soil, elasto-plastic bounding surface model is considered, which is a sophisticated elasto-plastic model for normally and over consolidated soils. The influence of loading intensity and consolidation process are considered carefully. The analyses showed that the elasto-plastic bounding surface model may provide a realistic stress distribution within the soil mass around the piles. Also as conclusion of a series of analyses, the followings are clarified; 1) the long-term behavior of two-pile group system; 2) the mechanism of how the space between piles affects the long-term displacements.

Keywords: Pile Group, Finite Element, Bounding Surface Model, Consolidation, Axial Loading, Lateral Loading, Combined Loading

تصرف الانضمام لاسس مجموعة ركائز مكونة من ركيزتين تحت حالات تحميل مختلفة بأستخدام نموذج لدن- مرن السطح المحيط

الخلاصة

في هذه الدراسة تم التحري عن التصرف الزمني لأسس مجموعة ركائز مكونة من رَكيزتين في الوسط المسامي المشبع تحت حالات تحميل مختلفة بأستخدام طريقة العناصر المحددة. هذا التصرف يحدث بسبب الأنضمام في الوسط المشبع. تم تمثيل التربة الطينية بأستخدام نموذج لدن- مرن السطح

https://doi.org/10.30684/etj.31.19A.14
2412-0758/

المحيط (elasto-plastic bounding surface model) وهي من النماذج المعقدة تستخدم لتمثيل تصرف الترب الطينية عالية وطبيعية الانضمام.

تملتاًحري عن تصرف نظام مجموعة ركائز مكونة من رَكيزتين تحت حالات تَحميل مُختلفة لدراسة تأثير التحميل, عملية الأنضمام والمسافات على الأزاحات و ضغط الماء المسام. أضهرت النتائج التي عُرِضت بأن النموذج اللدن- المرن السطح المحيط (elasto-plastic bounding surface model) يوفر توزيع واقعي للأجهاد في التربة حول الركائز. كذلك, لوحظ تأثير التحميل, عملية الأنضمام والمسافات على الأزاحات و توزيع زيادة ضغط الماء للمَسامات حولَ نظام المجموعة.

INTRODUCTION

In foundation engineering, generally the most popular types of foundations used for high rise buildings or special structures are pile foundations. With the development of the finite element method, the ability to numerically model complicated soil structure has become possible. Geotechnical construction is one such area that has been investigated extensively by the finite element method. The work presented in this study is concerned with one particular area of geotechnical construction, that of piles.

It is well known that the time-dependent behavior of soil deformation plays an important role in performance of major structures on soil foundation. The time-dependent behavior of soil results from both properties of viscosity and consolidation which display certain nonlinear characteristics. Time-dependent effects play an important role in the design and construction of pile.

It is generally accepted that the finite element method is the major technique used in numerical analysis of geotechnical problems particularly piles and soil consolidation. Therefore, the finite element will appear to offer a numerical technique which is suited to the task of analyzing time dependent behavior of piles in elasto-plastic soils, and during each stage of loading on pile, the excess pore pressure and deformation can be predicted.

In this study a finite element program has been modified to simulate time-dependent behavior of two-pile group system in saturated cohesive soils under lateral, axial and combined loadings. The nonlinear stress-strain behaviors of soils are modeled via bounding surface type plasticity, which allows the plastic displacement to occur for stress points within the surface. A parametric study is carried out to address the influence of various factors, such as load intensity, consolidation process and spacing on the prediction of time-dependent piled foundation behavior in several types of cohesive soils.

LINEAR ELASTIC MODEL OF PILE

This model represents Hooke's law of isotropic linear elasticity used for modeling the stress-strain relationship of the pile material. The model involves two elastic stiffness parameters, namely Young's modul

Figure (1). It is primarily used for modeling of stiff structural member for example piles in the soil.

Hooke's law can be given by the Eq. (1):

$$\begin{bmatrix}\sigma_{xx}\\ \sigma_{yy}\\ \sigma_{zz}\\ \sigma_{xy}\\ \sigma_{yz}\\ \sigma_{zx}\end{bmatrix}=\frac{E}{(1-2\upsilon)(1+\upsilon)}\begin{bmatrix}1-\upsilon & \upsilon & \upsilon & 0 & 0 & 0\\ \upsilon & 1-\upsilon & \upsilon & 0 & 0 & 0\\ \upsilon & \upsilon & 1-\upsilon & 0 & 0 & 0\\ 0 & 0 & 0 & \frac{1}{2}-\upsilon & 0 & 0\\ 0 & 0 & 0 & 0 & \frac{1}{2}-\upsilon & 0\\ 0 & 0 & 0 & 0 & 0 & \frac{1}{2}-\upsilon\end{bmatrix}\begin{bmatrix}\varepsilon_{xx}\\ \varepsilon_{yy}\\ \varepsilon_{zz}\\ \gamma_{xy}\\ \gamma_{yz}\\ \gamma_{zx}\end{bmatrix} \quad \ldots(1)$$

The relationship between Young's modulus *E* and other stiffness moduli, such as the shear modulus *G*, the bulk modulus *K*, and constrained modulus *M*, is given by:

$$G = \frac{E}{2(1+\upsilon)} \quad \ldots(2)$$

$$K = \frac{E}{3(1-2\upsilon)} \quad \ldots (3)$$

$$M = \frac{(1-\upsilon)E}{(1-2\upsilon)(1+\upsilon)} \quad \ldots (4)$$

BOUNDING SURFACE MODEL OF SOIL

The numerical implementation of the model and the parameters associated with the model are available in Dafalias and Herrmann, (1986) and Herrmann et al., (1987). The elasto-plastic rate relations are the total strain rate is consisting of two parts: elastic strain and plastic strain:

$$\dot{\varepsilon}_{ij} = \dot{\varepsilon}^{e}_{ij} + \dot{\varepsilon}^{p}_{ij} \quad \ldots (5)$$

Where a dot indicates a rate and an associated flow rule is assumed. The inverse form of the constitutive relations is obtained as:

$$\dot{\sigma}_{ij} = D_{ijkl}\,\dot{\varepsilon}_{kl} \quad \ldots (6)$$

$$D_{ijkl} = G\left(\delta_{ki}\delta_{lj} + \delta_{kj}\delta_{li}\right)\cdot\left(K - \frac{2}{3}G\right)\delta_{ij}\delta_{kl} - \frac{\bar{h}(L)}{B}\left[3KF_{,I}\delta_{ij} + \frac{G}{J}F_{,J}s_{ij} + \frac{\sqrt{3}G}{\cos(3\alpha)}\frac{F_{,\alpha}}{bJ}\left(\frac{s_{in}s_{nj}}{J^2} - \frac{3S^3 s_{ij}}{2J^4} - \frac{2\delta_{ij}}{3}\right)\right]\left[3KF_{,I}\delta_{kl} + \frac{G}{J}F_{,J}s_{kl} + \frac{\sqrt{3}G}{\cos(3\alpha)}\frac{F_{,\alpha}}{bJ}\left(\frac{s_{kn}s_{nl}}{J^2} - \frac{3S^3 s_{kl}}{2J^4} - \frac{2\delta_{kl}}{3}\right)\right] \quad \ldots (7)$$

Where:

$$L = \frac{1}{B}\left\{3KF_{,I}\dot{\varepsilon}_{kk} + \frac{G}{J}F_{,J}s_{ij}\dot{\varepsilon}_{ij} + \frac{\sqrt{3}G}{\cos(3\alpha)}\frac{F_{,\alpha}}{bJ}\left[\left(\frac{s_{ik}s_{kj}}{J^2} - \frac{3S^3 s_{ij}}{2J^4}\right)\dot{\varepsilon}_{ij} - \frac{2\dot{\varepsilon}_{kk}}{3}\right]\right\} \quad \ldots (8a)$$

$$B = K_p + 9K(F_{,I})^2 + G(F_{,J})^2 + G\left(\frac{F_{,\alpha}}{bJ}\right)^2 \quad \ldots (8b)$$

and where K and G represent the elastic bulk and shear moduli, respectively; δ_{ij} is the Kronecker delta; K_p the plastic modulus; I , J and α are the stress invariants; $1 \leq b \leq \infty$ and F represents the analytical expression of the bounding surface; s_{ij} represents the deviatoric part of the stress tensor and $S^3 = (s_{ij}s_{jk}s_{ki})/3$ represents the third deviatoric stress invariant.

FORMS OF THE BOUNDING SURFACE

The analytical definition of the bounding surface may assume many particular forms provided it satisfies certain requirements concerning the shape of the surface (Dafalias and Herrmann, 1986). The analytical expressions for a composite form of the bounding surface, consisting of two ellipses and one hyperbola, with continuous tangents at their connecting points (Figure, 2), are presented below (Dafalias and Herrmann, 1986).

For ellipse 1:

$$F = (\bar{I} - I_o)\left(\bar{I} + \frac{R-2}{R}I_o\right) + (R-1)^2\left(\frac{J}{N}\right)^2 = 0 \quad \ldots (9)$$

For the hyperbola:

$$F = \left(\bar{I} - \frac{I_o}{R}\right)^2 - \left(\frac{I}{N} - \frac{I_o}{R}\right)\left[\frac{I}{N} - \frac{I_o}{R}\left(1 + 2\frac{RA}{N}\right)\right] = 0 \qquad \ldots (10)$$

For ellipse 2:

$$F = (\bar{I} - TI_o)[\bar{I} - (T + 2\xi)I_o] + \rho\bar{J}^2 = 0 \qquad ...(11a)$$

Where:

$$\xi = -\frac{T(Z+TF')}{Z+2TF'},\ \rho = \frac{T^2}{Z(Z+TF')} \qquad \ldots (11b)$$

$$F' = \frac{N}{\sqrt{1+y^2}},\quad y = \frac{RA}{N},\ \bar{I} = \frac{N}{R}\left(1 + y - \sqrt{1+y^2}\right) \qquad \ldots (11c)$$

Elasto-Plastic Bounding Surface Model Parameters

The parameters are divided into the following three groups (Kaliakin, 2005):

Traditional material constants

λ = slope of consolidation line,
κ = slope of swelling line,
$N(\alpha)$ = slope of critical state line, $N_c = N$ in compression, $N_e = N$ in extension,
υ= Poisson's ratio.

Surface configuration parameters

$R(\alpha) = R > 1$defines the point $I_1 = I_\circ/R$ Figure (2), which together with point J_1 defines the coordinates of point H which is the intersection of $F = 0$ and CSL, $R_c = R$ in compression, $R_e = R$ in extension, shape parameter determine the ratio of the major to minor axis of ellipse 1 ($2.0 \leq R \leq 3.0$),$A(\alpha)$ = parameter defines the distance $D = AI_\circ$ of apex H of the hyperbola from its center G intersection of the two asymptotes and thus pertains only to the composite form of the surface, Ac=A in compression, Ae=A in extension, shape parameter controls the shape of the hyperbolic portion of the bounding surface ($0.02 \leq A \leq 0.2$),T = It /I◦ parameter which determines the purely tensile strength of the material, and T also pertains to the composite form of the surface, C = $0 \leq C < 1$ parameter which determines the center of the bounding surface Ic= CI◦. The projection center parameter ($0 \leq C \leq 1$) defines the point along the I-axis which serves as the projection center in the radial mapping rule

Hardening parameters

s_p = parameter which determines indirectly "elastic nucleus". For $s_p = 1$ the elastic nucleus degenerates to point I_c center of bounding surface and as $s_p \to \infty$ the elastic nucleus expands towards the bounding surface.

h = slope-hardening factor, which is a function of lode angle (α), h_c= for compression $(h_c = h(\pi/6))$, h_e =for extension $(h_e = h(-\pi/6))$

a and w = hardening parameters if the single ellipse version of the bounding surface is used.

m= a positive model parameter.

Finite Element Formulation

The elasto-plastic bounding surface model described above is incorporated in a finite element program, which has the feature of modeling two-dimensional (plane strain and axisymmetric) geotechnical problems such as consolidation, written by FORTRAN90 language. This program is primarily based on the programs presented by Smith and Griffiths (2004) for the analysis of two-dimensional solid by finite element method utilizing elastic constitutive relationship and which is modified for the purpose of this study.

The program is modified to take into consideration consolidation process, linear elastic model for representing the pile material and the elasto-plastic bounding surface and Mohr-Coulomb models for representing the soil surrounding the pile. So in addition to the elasto-plastic bounding surface model, the modified program allows one to assign linear elastic behavior and Mohr-Coulomb failure criterion to any part of the problem geometry. Description of all of the program features is beyond the scope of this paper, and a brief summary of the feature relevant to this study is given below.

Transient Formulation

In the case of a pile in saturated porous medium, the loading is time-dependent, so an incremental formulation was used in the following work producing the matrix version of the Biot equation at the element level presented below *(Lewis and Schrefler, 1987).*

$$\begin{bmatrix} K & L \\ L^T & S+\bar{\alpha}H\Delta t_k \end{bmatrix}\begin{Bmatrix} \bar{u} \\ \bar{p} \end{Bmatrix} = \begin{bmatrix} K & L \\ L^T & S-(1-\bar{\alpha})H\Delta t_k \end{bmatrix}\begin{Bmatrix} \bar{u} \\ \bar{p} \end{Bmatrix} + \begin{Bmatrix} dF/dt+C \\ \bar{F} \end{Bmatrix} \quad \ldots (12)$$

where: K =element solid stiffness matrix, L =element coupling matrix, H =element fluid stiffness matrix, $\bar{u}$ =change in nodal displacements, $\bar{p}$ =change in nodal excess pore-pressures, S =the compressibility matrix, $\bar{F}$ =load vector, Δt =calculation time step, $\bar{\alpha}$=time stepping parameter (=1 in this work), dF/dt =change in nodal forces.

VALIDATION OF NUMERICAL MODELS

Consolidated undrained triaxial compression for normally consolidated clay

This problem has been drawn from Herrmann et al., (1981), as reported by Dafalias and Herrmann (1986). Laboratory-prepared Kaolin clay was tested and the measured data are taken from the latter authors, whereas the composite bounding surface model parameters are taken from the former. The values of parameters are listed in Table (1).

The model behavior against the experimental data is illustrated in Figure (3). The results indicate that the model successfully predicts results for normally consolidated clays under compression loadings in undrained condition.

Consolidated undrained triaxial compression for over-consolidated clay

The problem is drawn from Banerjee and Stipho (1979) and the test data are simulated using the input parameters listed in Table (2). Also, the model parameters

are taken from Dafalias and Herrmann (1982) with the overconsolidation ratio (OCR) equal five.

The model behavior against the experimental data is illustrated in Figure (4). And as for normally consolidated clay, the results also indicate that the model successfully predicts results for over-consolidated clays under compression loadings in undrained condition.

Time-Dependent Behavior of Two-Pile Group System Using Bounding Surface Model

A time-dependent behavior of two-pile group system with diameter D_p= 1m, length of pile= 10m and cap of thickness =0.5m is studied in this section. The pile group is embedded in layer of saturated elasto-plastic cohesive soil which obeys the bounding surface model, Grenoble soil is used, the parameters are presented in Table (3). Also parameters used for elastic model representing cap are the same used for concrete pile material tabulated in Table (4). The two-pile group system will be subjected to lateral, axial and combined loading applied at the centre of the cap. For friction piles the spacing centre to centre should be not less than the perimeter of the pile or, for circular piles, three times the diameter (*British standard, 1986*), therefore the spacing between the two piles is taken as $3D_p$. The problem is analyzed assuming elastic model for pile and cap material and elasto-plastic bounding surface model for soil surrounding the pile. The finite element mesh and dimensions of the problem are shown in Figure (5).

Influence of Loading and consolidation process

In the elasto-plastic analysis, the lateral displacements are computed under lateral loading varied from $H=5\gamma_w\times D_p^3$ to $H=60\gamma_w\times D_p^3$ and the axial displacements are computed under axial loading varied from $V=5\gamma_w\times D_p^3$ to $V=100\gamma_w\times D_p^3$ applied at the center of the cap. Also, the lateral and axial displacements are computed under combined loading with load ratios of V/H=4, V/H=10 and V/H=20 applied at the center of the cap. The computations are carried out for time factors of Tv= 0.0001, 0.1, and 1.0. The excess pore water pressure (EPWP in kPa) distribution around and below the pile group system will be investigated too under the influence of highest lateral, axial and combined loading for the three time factors.

Lateral displacements of the piles with depth in the two-pile group system under lateral loading H=5, 35 and $60\gamma w\times D_p^3$ are plotted in Figures (6a, 6b and 6c) respectively. These figures show that the lateral displacements for the two piles are increasing with time and loading, but the influence of time (i.e, consolidation process) will vanish gradually with depth and being insignificant at the base of pile. At a time

factor T_v= 0.0001, the lateral displacements of pile (1) under the three loading are smaller than the lateral displacements of pile (2) with almost equal head displacement, while at time factors T_v= 0.1 and 1.0, the displacements for the two piles are approximately the same the with higher pile (1) head displacement of about 5% . Also the percentage of increase in piles head displacement during the consolidation process range between 45% to 50% of the value at the time factor T_v=0.0001. Such increasing in displacements with time are due to the dissipation of excess pore water pressures Which are generated and concentrated in the vicinity of upper parts of piles and in between with zero values below and around base of piles. The concentration of the irregular distribution of EPWP is higher in front of pile (1) than pile (2) which is being regular with time and as shown in Figures (7a, 7b and 7c) that show the contours of EPWP around piles under higher lateral loading $H=60\gamma_w \times Dp_3$ for the three time factors T_v=0.0001, 0.01 and 1.0, respectively. With time interval, the dissipation is in higher rate near the heads of the piles and in between. At time factor T_v=1.0 the EPWP values near head of pile is lower than that near the base being increased away from piles and remains zero below them.

Figures (8a, 8b and 8c) shows the axial displacements of the piles with depth in the two-pile group system under axial loading V=5, 50 and $100\gamma w \times Dp^3$, respectively. It has been observed that the axial displacements for the two piles with depth are equal and a small difference between them is noticed at the beginning of consolidation time due to irregular distribution of EPWP which is regular with time. The axial displacements are increased with loading and time, and the influence of consolidation process appears to be almost in a same rate with depth taking in consideration that the increasment of pile head axial displacement with time is in a range of 50% to 55% from those values at the beginning of consolidation time. Such higher displacement of pile with time is due to dissipation of EPWP around the piles and as shown in Figures (9a, 9b and 9c) which illustrate the EPWP distribution around piles under higher axial loading $V=100\gamma_w \times D_p^3$ for the three time factors T_v=0.0001, 0.01 and 1.0, respectively.

The dissipation will be expected in a higher rate in the upper parts of piles and in between being concentrated below and around the base of piles.

Figures (10a, 10b and 10c) show the lateral displacements of the piles with depth in the two-pile group system under combined loading V/H=4, 10 and 20, respectively. The indication under combined load is obtained here that axial load has more effects on the behavior of piles than lateral load and this influence being more noticeable with increasing load ratio and time. Also the values for lateral displacements of pile (1) are higher than that for pile (2) under all load ratios.

Figures (11a, 11b and 11c) show axial displacement of piles with depth under the load ratios V/H=4, 10 and 20, respectively. It can be seen that axial displacements of piles are increased with load ratios and time, and the axial displacements of pile (1) with depth are higher than pile (2) may be due to bending effect together with loading and such difference in displacements can be disappeared gradually with time and load ratios.

Figure (12a) depicts the contours of EPWP around the piles at the beginning of consolidation time. The increase in the lateral and axial displacements discussed above may be due to dissipation of the EPWP values with time and as presented in Figures (12b and 12c) which show the distribution of EPWP at the time factors T_v=0.1 and T_v=1.0, respectively.

Influence of Spacing

In order to study the influence of the spacing between the centres of piles on the time-dependent behavior of the two-pile group system, the spacing between the two piles is increased from $3D_p$ to $4D_p$. The finite element mesh and dimensions of the problem are shown in Figure (13). Also the displacements and excess pore water pressure distribution around and below the pile group system have been investigated under the influence of highest lateral, axial and combined loading for the three time factors T_v=0.0001, 0.01 and 1.0.

Figures (14 and 15) show the lateral displacements with depth of piles (1) and (2), respectively under lateral loading $H=60\gamma w\times D_p^3$ for $3D_p$ and $4D_p$ spacing, Figures (16) and (17) show the axial displacements with depth of piles (1) and (2), respectively under axial loading $V=100\gamma w\times D_p^3$ for $3D_p$ and $4D_p$ spacing, Figures (18) and (19) show the lateral displacements with depth of piles (1) and (2), respectively under combined loading of load ratio V/H=20 for $3D_p$ and $4D_p$ spacing and Figures (20 and 21) show the axial displacements with depth of piles (1) and (2), respectively under combined loading of load ratio V/H=20 for $3D_p$ and $4D_p$ spacing. The results from figures above show that the amount of displacements decreases when the space between piles increases, while the behaviors of long-term displacement are almost the same. This can be attributed to the fact that the displacements of pile foundation are accompanied with the change of the load sharing rate, and the mechanism of this phenomenon may be clarified as follows; 1) piles obtain enough frictional force because the soil is less restrained between piles; 2) EPWP exists in a higher percentage between the piles and the consolidation of clay (i.e, dissipation of EPWP) delays around and/or below piles and as indicated in Figures (22, 23 and 24) which show the EPWP distribution for $4D_p$ spacing under lateral, axial and combined loading, respectively. This phenomenon cannot be found in the case of single pile, this problem is peculiar to the pile foundation (= Pile Group Effect). In the current research, it is well-known that the influence of pile group effect closely relates to the space between piles. Also from figures it has been indicated that influence of spacing is more noticeable on pile (1) than pile (2).

It should be noticed that when the space between piles decreases, frictional force obtained from ground also decreases, and stress transmitted by pile end increases. Also the interaction of pile-soil-pile system is emphasized by decreasing in the space between piles, and pile group should behave like single caisson when the space between piles is narrow. In addition, the concentration of the stress transmitted by pile end is emphasized.

CONCLUSIONS

1. The analyses showed that the elasto-plastic bounding surface model may provide a realistic stress distribution within the soil mass around the piles.
2. The maximum displacement appeared at the head of pile decreasing with the depth and the lower loading, also there appear to be significant influence of time (i.e., consolidation process) on the displacements.
3. The EPWP distribution is irregular at the beginning time of consolidation became more regular with time; also the long term dissipation will be in higher rate near the head of the pile. With time the EPWP values near head of pile will be lower than that near the base being increased away from piles.
4. The axial displacements of piles increases with load ratios and time, and the axial displacements of pile (1) with depth are higher than pile (2), knowing that such difference in displacements has been disappeared gradually with time and load ratios.
5. The results show that the amount of displacements decreases when the space between piles increases and the behaviors of long-term displacement are almost the same. Also the EPWP exist in a higher percentage between the piles with larger spacing and the consolidation of clay (i.e, dissipation of EPWP) delays around and/or below piles.

REFERENCES

[1]. Banargee, P. K., and Stipho, A. S., (1979), "An Elasto-Plastic Model for Undrained Behavior of Heavily Overconsolidation Clays", Short Communication, International Journal for Numerical and Analytical Methods in Geomechanics, Vol.3, pp. 97-103.

[2]. BS 8004-1986, "Code of Practice for Foundations (Formerly CP 2004)", British Standard, Section 7.3.4.2, pp. 114.

[3]. Dafalias, Y. F., and Herrman, L.R., (1982), "Bounding surface Formulation of Soil Plasticity", Soil Mechanics-Transient and Cyclic loads, Eds., Pande, G.N., and Zienkinwics, O.C., John Wiley and Sons, pp. 253-282.

[4]. Dafalias, Y. F., and Herrmann, L. R., (1986), "Bounding Surface Plasticity II: Application to Isotropic Cohesive Soils", Journal of Engineering Mechanics, ASCE, Vol.112, No.12, pp. 1263-1291.

[5]. Herrmann, L. R., Shen, C. K., Jafroudi, S., DeNatale, J. S., and Dafalias, Y. F., (1981), "A Verification Study for the Bounding Surface Plasticity Model for Cohesive Soils", A Report. Department of Civil Engineering, University of California, Davis, USA.

[6]. Herrmann L. R., Kaliakin V. N., Shen C. K., Mish K. D., and Zhu Z., (1987), "Numerical Implementation of Plasticity Model for Cohesive Soils", Journal of Engineering Mechanics. Vol.113, No.4, pp. 500-519.

[7]. Johnson, K., Lemcke P., Karunasena W. and Sivakugan N., (2006), "Modelling the Load Deformation Response of Deep Foundation under Oblique Loading", School of Engineering, James Cook University, Townsville, Queensland, 4811, Australia,
Environmental Modeling and Software Vol. 21, Issue 9, September 2006, pp. 1375-1380.

[8]. Kaliakin, V. N., and Dafalias, Y. F., (1991) "Details Regarding the Cohesive Soils", Civil Engineering Report No.91-1, University of Delaware, Newark.

[9]. Kaliakin V.N., (2005), "Parameter Estimation for Time-Dependent Bounding Surface Models". Geo-Frontiers Conference (2005); Soil Constitutive Models: Evaluation, Selection, and Calibration. Geotechnical special publication, No.128, pp. 237-256.

[10]. Lewis, R. W., and Schrefler, B. A., (1987), "The Finite Element Method in the Deformation and Consolidation of Porous Media", John Wiley and Sons, Ltd., London.

[11]. Smith, I. M., and Griffiths, D. V., (2004), "Programming Finite Element Method", 4th Ed., John Wiley and Sons.

Table (1) Bounding surface parameters for normally consolidate clay (undrained triaxial compression) (after Dafalias and Herrmann, 1986).

Parameters	*Values*	*Parameters*	*Values*	*Parameters*	*Values*
P_o	***392.2***	M_e	***___a***	C	***0.07***
e_{in}	***0.63***	R_c	***2.5***	s_p	***1.0***
	0.15	R_e	***a***	h_c	***50.0***
	0.018	A_c	***0.02***	h_e	***a***
	0.3	A_e	***a***	a	***b***
M_c	***1.25***	T	***-0.1***	w	***___b***

[a] **Material response in extension was not simulated**

[b] **A bounding surface consisting of two ellipses and a hyperbola was used; this parameter does not enter into the formulation.**

Table (2) Bounding surface model parameters for overconsolidated clay (after Dafalias and Herrmann, 1982).

Parameters	*Values*	*Parameters*	*Values*	*Parameters*	*Values*
P_o	***414.0***	M_e	***1.05***	C	***0.0***
e_{in}	***0.94***	R_c	***2.72***	s_p	***1.0***
	0.14	R_e	***c***	h_c	***44.0***
	0.05	A_c	***___c***	h_e	***44.0***
	0.15	A_e	***c***	a	***1.2***
M_c	***1.05***	T	***___c***	w	***5.0***

[c] **A bounding surface consisting of a single ellipse was used in the analysis; this parameter is not used in this form of the model.**

Table (3) Bounding surface parameters for Gernoble cohesive soil (after Kaliakin and Dafalias 1991).

Properties / *Soil type*				M_c	M_e	R_c	R_e	A_c	A_e	C	h_c	h_e
Grenoble	*0.2*	*0.1*	*0.15*	*0.78*	*0.8*	*2.5*	*2*	*0.02*	*0.02*	*0.5*	*4.3*	*4.3*

Table (4) Properties for pile material (After Carter and Taibat, 2001).

Properties	*Values*
γ_c, *unit weight, kN/m*^{3}	*24.0*
υ, *Poisson's ratio*	*0.2*
E_p, *modulus of*	*30*10*^{6}

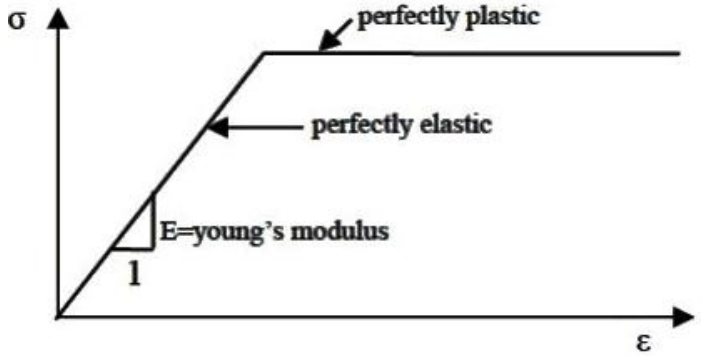

Figure (1) stress-strain curve (Johnson, et. al. 2006).

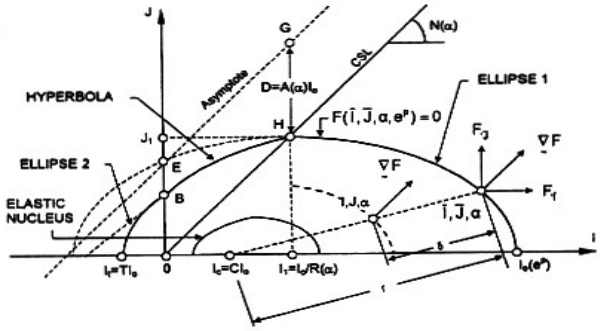

Figure (2) Bounding surface in stress invariants space (After Dafalias and Herrmann, 1986).

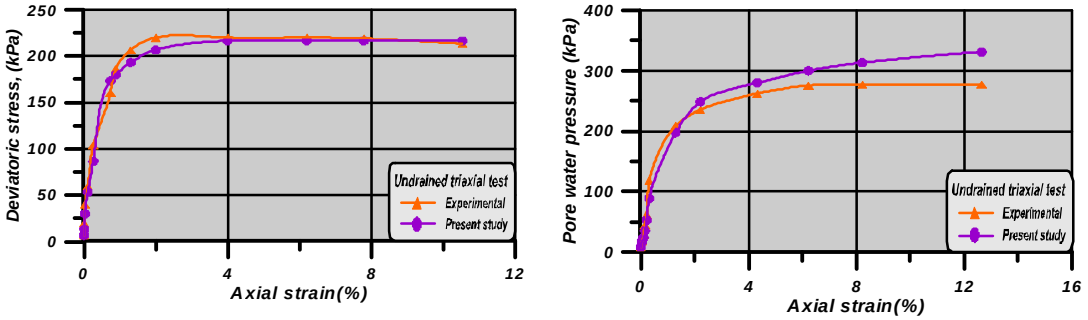

Figure (3) Simulation of consolidated undrained triaxial compression response of normally consolidated clay.

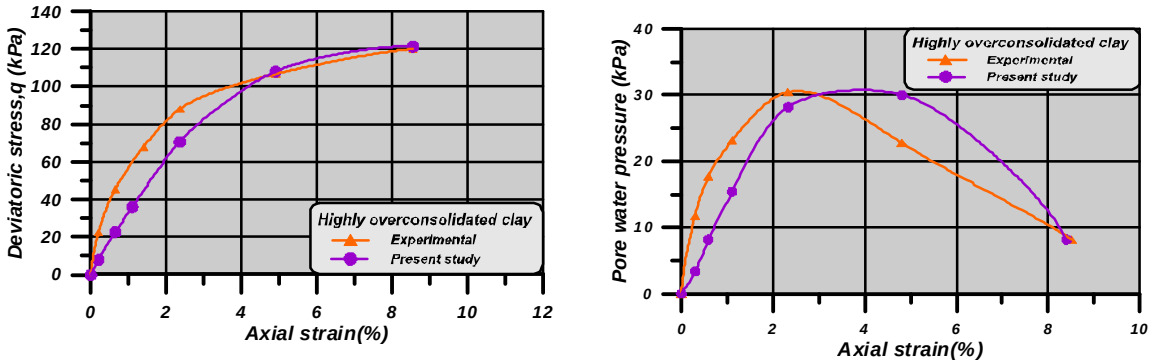

Figure (4) Simulation of consolidated undrained triaxial compression response of over-consolidated clay.

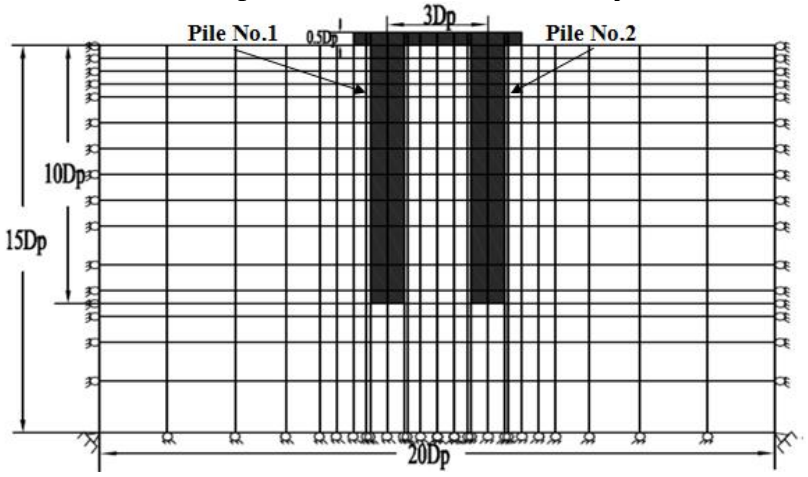

Figure (5) Finite element mesh.

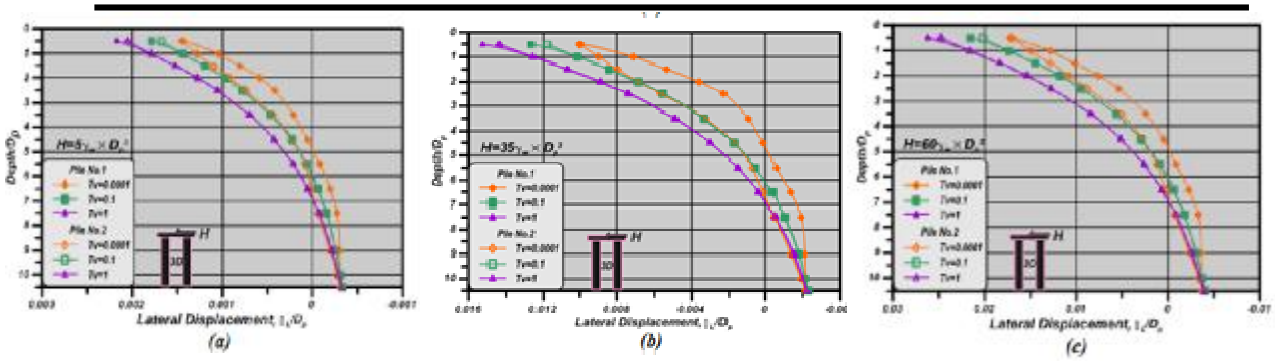

Figure (6) Lateral displacement of two piles with depth under lateral loading (a) ($H=5\gamma_w\times D_p^3$); (b) ($H=35\gamma_w\times D_p^3$) and (c) ($H=60\gamma_w\times D_p^3$).

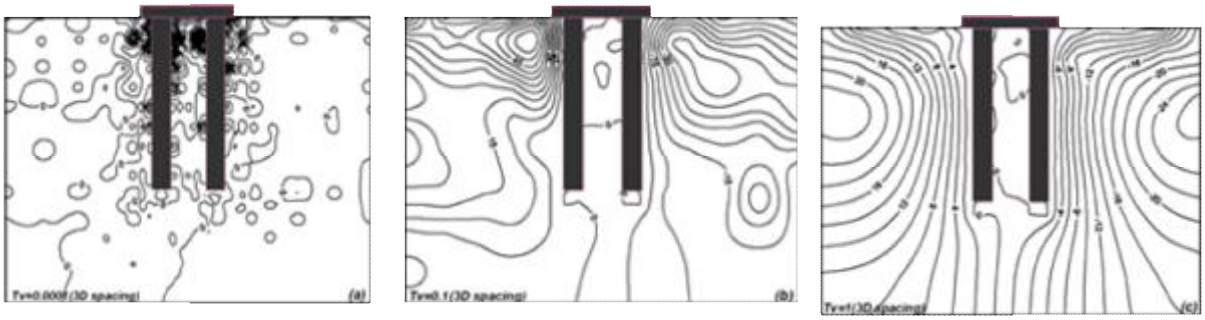

Figure (7) EPWP for $3D_p$ spacing under lateral loading.

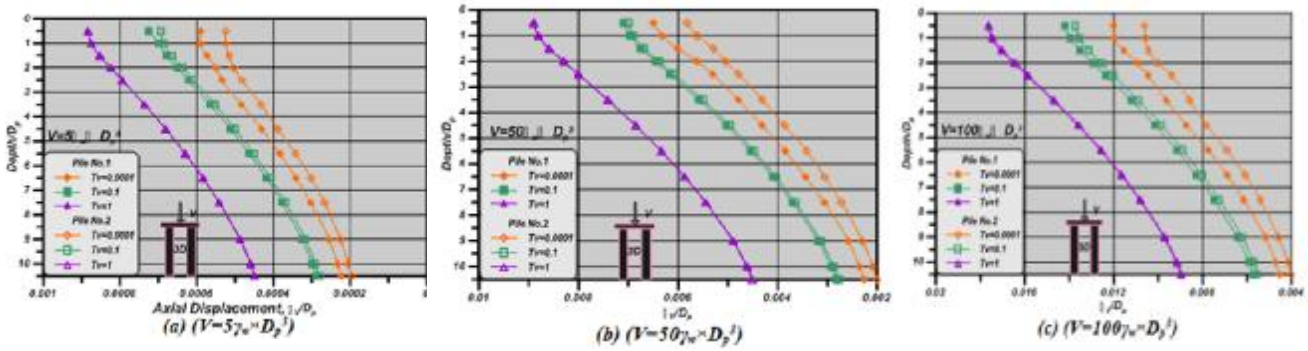

Figure (8) Axial displacement of two piles with depth under axial loading.

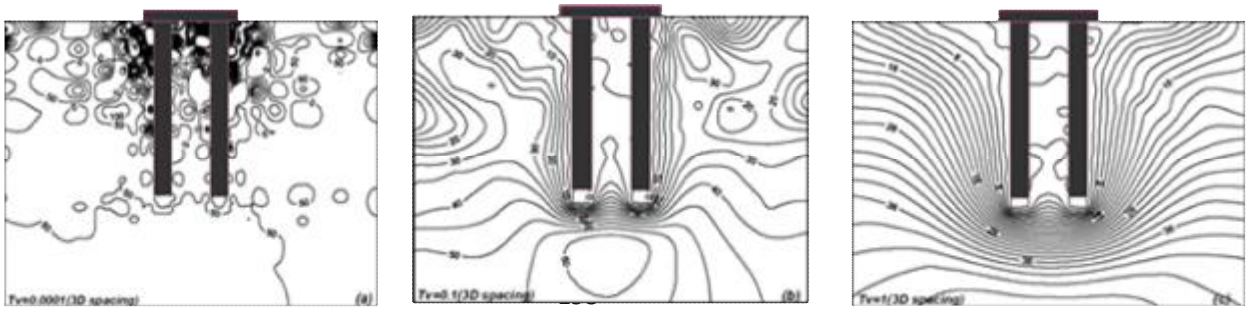

Figure (9) EPWP for $3D_p$ spacing under axial loading.

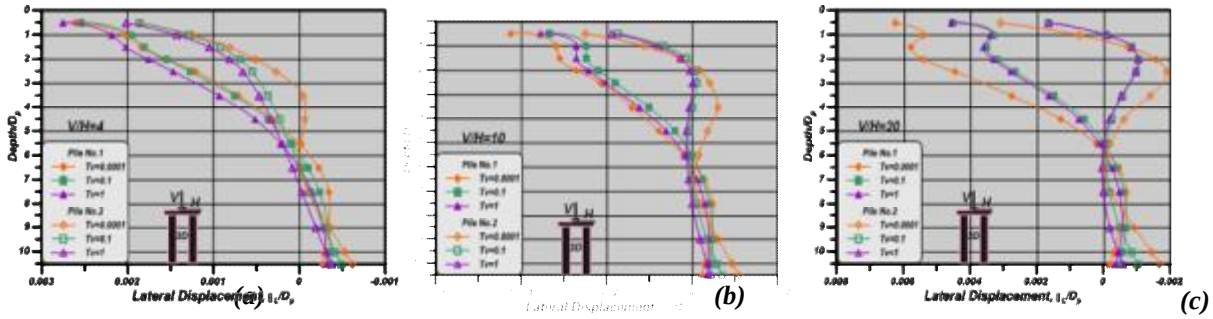

Figure (10) Lateral displacement of two piles with depth under combined loading (a):(V/H=4), (b):(V/H=10), (c):(V/H=20).

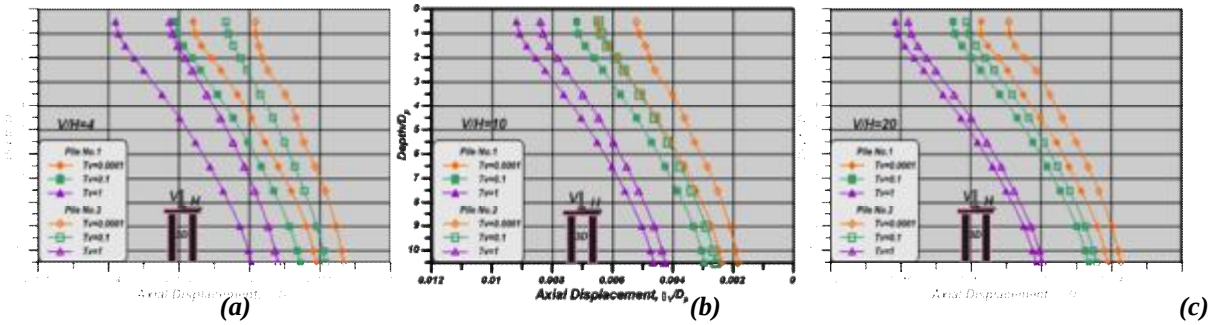

Figure (11) Axial displacement of two piles with depth under combined loading (a):(V/H=4), (b):(V/H=10), (c):(V/H=20).

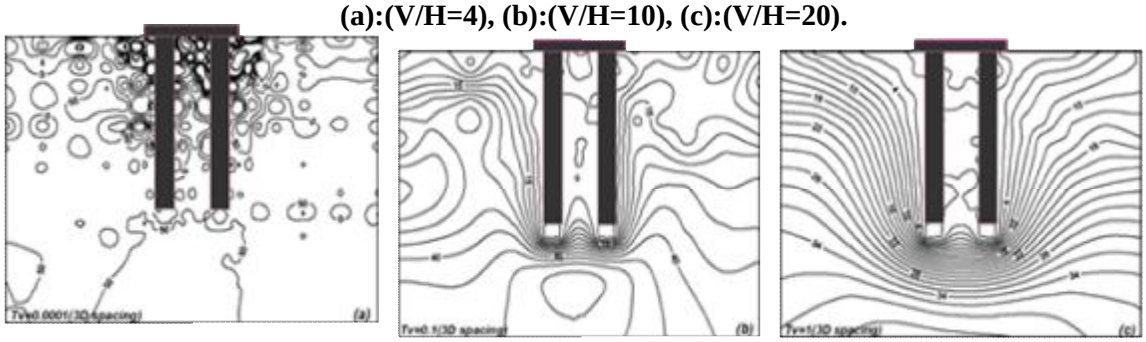

Figure (12) EPWP for $3D_p$ spacing under combined loading.

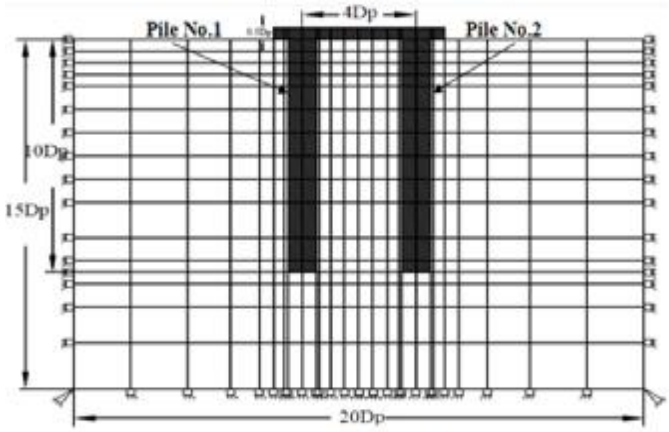

Figure (13) Finite element mesh for 4D$_p$ space.

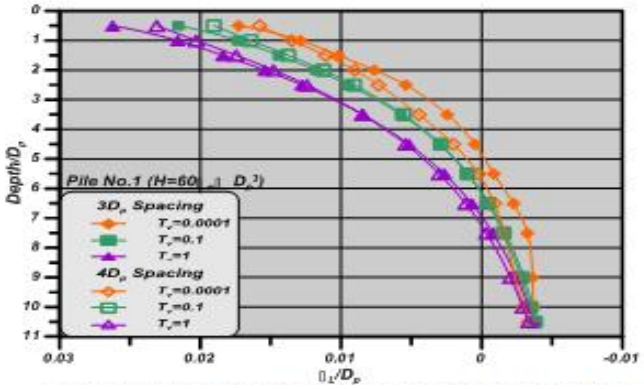

Figure (14) Lateral Displacement under lateral loading for Pile No.1 (3Dp and 4Dp spacing)

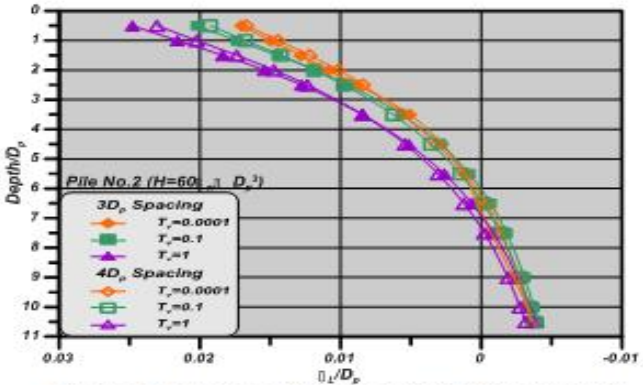

Figure (15) Lateral Displacement under lateral loading for Pile No.2 (3Dp and 4Dp spacing)

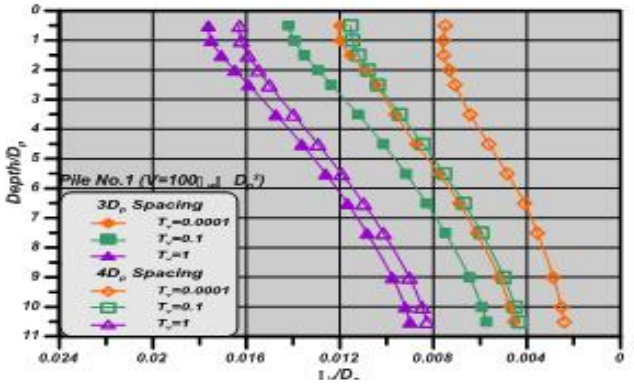

Figure (16) Axial Displacement under lateral loading for Pile No.1 (3Dp and 4Dp spacing)

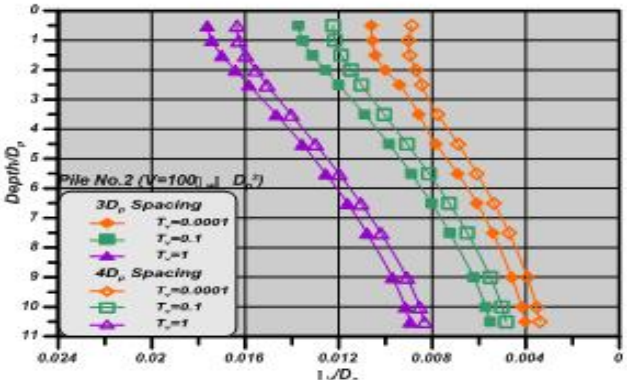

Figure (17) Axial Displacement under lateral loading for Pile No.2 (3Dp and 4Dp spacing)

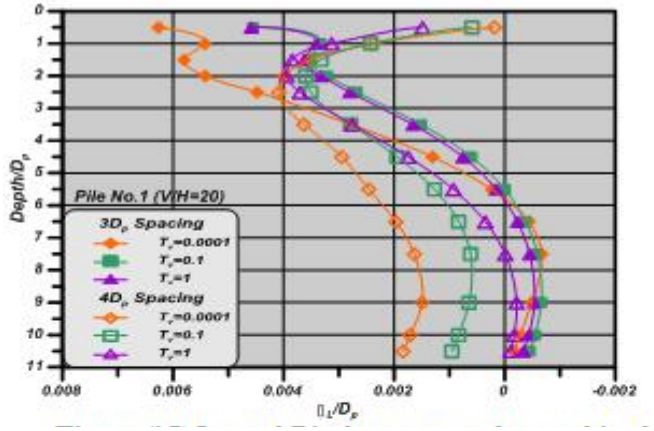

Figure (18) Lateral Displacement under combined loading for Pile No.1 (3Dp and 4Dp spacing)

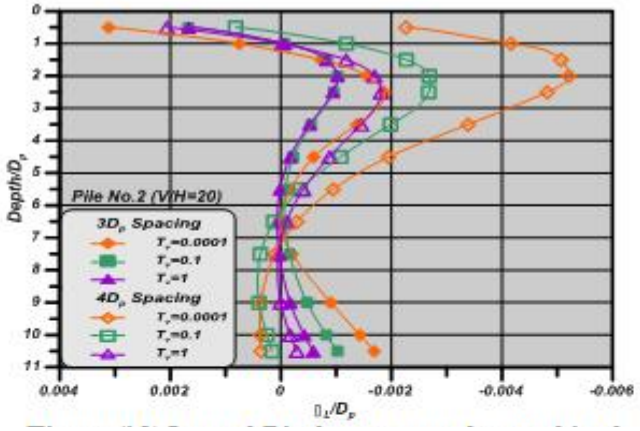

Figure (19) Lateral Displacement under combined loading for Pile No.2 (3Dp and 4Dp spacing)

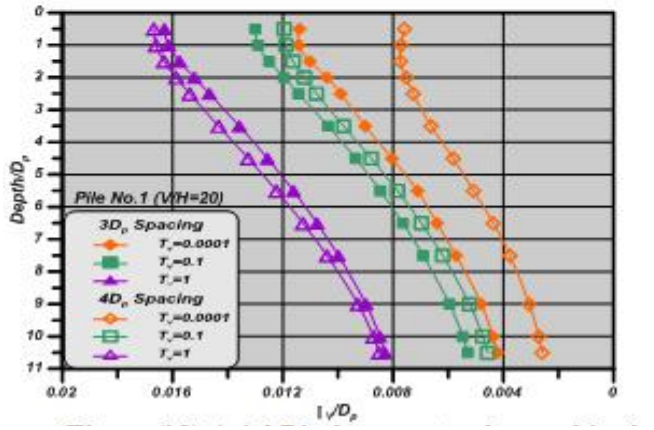

Figure (20) Axial Displacement under combined loading for Pile No.1 (3Dp and 4Dp spacing)

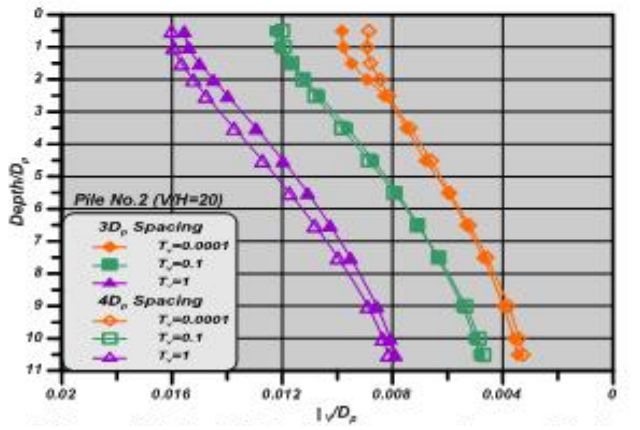

Figure (21) Axial Displacement under combined Loading for Pile No.2 (3Dp and 4Dp spacing)

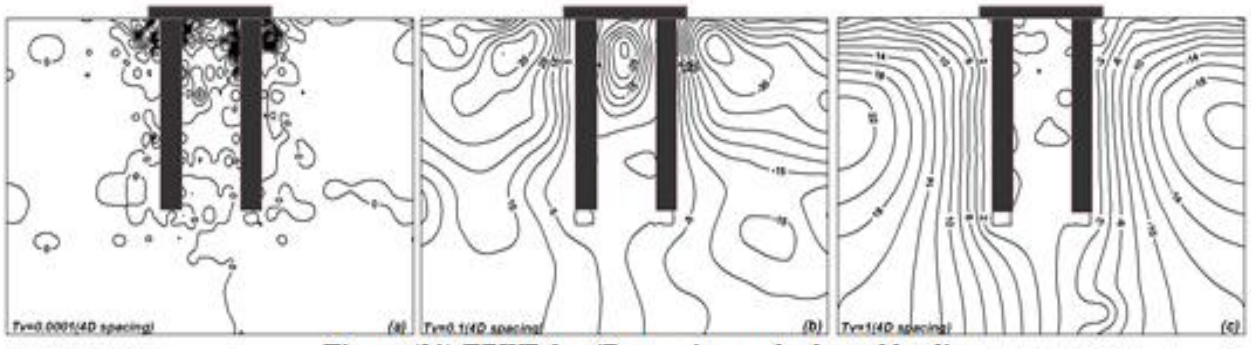

Figure (22) PWP for 4Dp spacing under lateral loading.

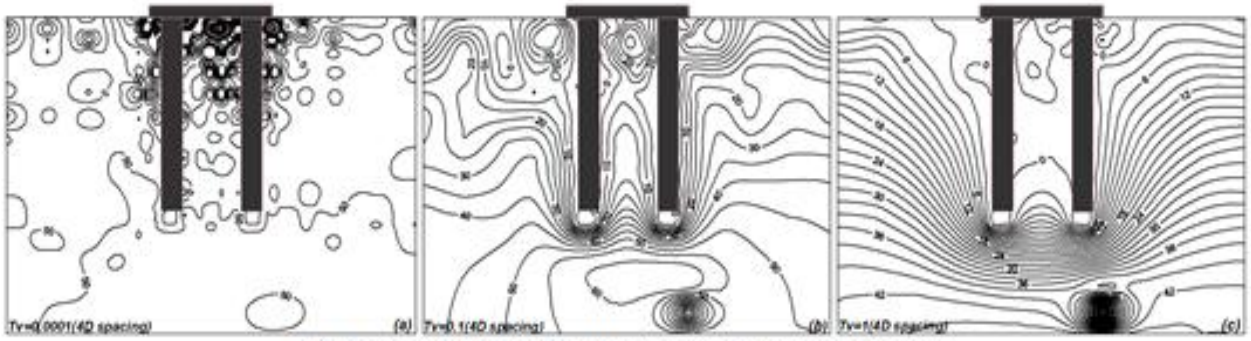

Figure (23) PWP for 4Dp spacing under axial loadin*g*.

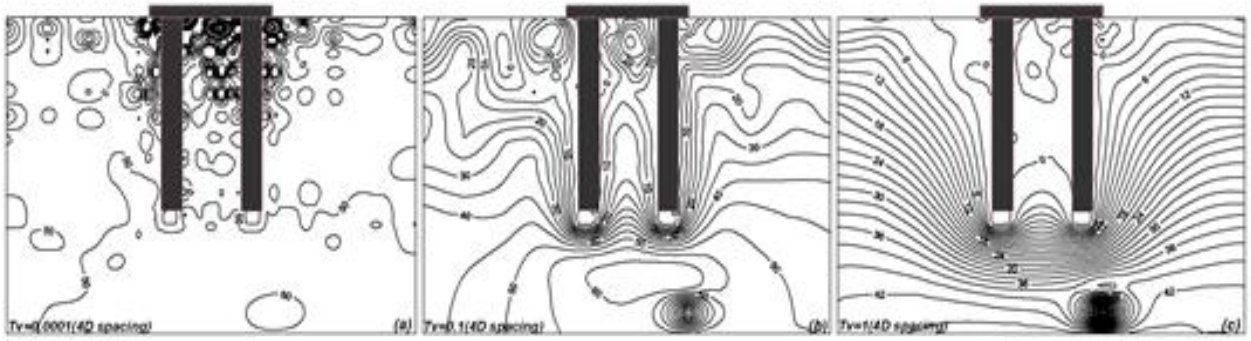

Figure (24) PWP for 4Dp spacing under combined.